Monthly Notices
of the
ROYAL ASTRONOMICAL SOCIETY

MNRAS **486,** 4334–4347 (2019)
Advance Access publication 2019 April 18

doi:10.1093/mnras/stz1108

AT 2017fvz: a nova in the dwarf irregular galaxy NGC 6822

M. W. Healy [1]★ M. J. Darnley [1]★ C. M. Copperwheat,[1] A. V. Filippenko,[2,3] M. Henze,[4] J. C. Hestenes,[2] P. A. James,[1] K. L. Page,[5] S. C. Williams [6] and W. Zheng[2]

[1]*Astrophysics Research Institute, Liverpool John Moores University, Liverpool L3 5RF, UK*
[2]*Department of Astronomy, University of California, Berkeley, CA 94720-3411, USA*
[3]*Miller Senior Fellow, Miller Institute for Basic Research in Science, University of California, Berkeley, CA 94720, USA*
[4]*Department of Astronomy, San Diego State University, San Diego, CA 92182, USA*
[5]*X-Ray and Observational Astronomy Group, Department of Physics & Astronomy, University of Leicester, Leicester LE1 7RH, UK*
[6]*Physics Department, Lancaster University, Lancaster LA1 4YB, UK*

Accepted 2019 April 15. Received 2019 April 15; in original form 2018 November 13

ABSTRACT

A transient in the Local Group dwarf irregular galaxy NGC 6822 (Barnard's Galaxy) was discovered on 2017 August 2 and is only the second classical nova discovered in that galaxy. We conducted optical, near-ultraviolet, and X-ray follow-up observations of the eruption, the results of which we present here. This 'very fast' nova had a peak V-band magnitude in the range $-7.41 > M_V > -8.33$ mag, with decline times of $t_{2,V} = 8.1 \pm 0.2$ d and $t_{3,V} = 15.2 \pm 0.3$ d. The early- and late-time spectra are consistent with an Fe II spectral class. The H α emission line initially has a full width at half-maximum intensity of $\sim$2400 km s^{-1} – a moderately fast ejecta velocity for the class. The H α line then narrows monotonically to $\sim$1800 km s^{-1} by 70 d post-eruption. The lack of a pre-eruption coincident source in archival *Hubble Space Telescope* imaging implies that the donor is a main-sequence, or possibly subgiant, star. The relatively low-peak luminosity and rapid decline hint that AT 2017fvz may be a 'faint and fast' nova.

Key words: stars: individual: (AT 2017fvz) – novae, cataclysmic variables.

1 INTRODUCTION

Classical novae (CNe) belong to the class of accreting binaries known as cataclysmic variables. As first proposed by Walker (1954), these are closely interacting binaries consisting of a white dwarf (WD) accreting material from a donor – either a main-sequence, subgiant, or red giant star (see Darnley et al. 2012). Through Roche lobe overflow or the stellar wind of an evolved donor, hydrogen-rich material from the donor streams, usually via an accretion disc (Warner 1995), on to the WD where severe heating and compression take place. Given favourable conditions, this results in a thermonuclear runaway (TNR) within the accreted envelope on the WD with a proportion of that envelope subsequently ejected – the nova eruption (Starrfield, Sparks & Truran 1976). The luminosity of these systems typically increases to a few $\times 10^4$ L$_\odot$ (see e.g. Bode 2010) with peak absolute magnitudes reaching $M_V \approx -10.5$ in extreme cases (Shafter et al. 2009; Aydi et al. 2018).

Following the TNR, stable H-burning continues within any material remaining on the WD surface. This results in the emission of a large amount of X-rays typically peaking in the range 30–50 eV – the so-called supersoft X-ray source (SSS; see van den Heuvel et al. 1992). The SSS is initially obscured by optically thick ejecta surrounding the nova; however, once the optical depth has decreased sufficiently, the SSS is unveiled.

All novae are predicted to recur (Yaron et al. 2005), but the broad range of times between consecutive eruptions has led to segregation based on recurrence period ($P_{\rm rec}$). CNe have been observed to erupt just once. Recurrent novae (RNe) are systems with a high-mass WD and high accretion rates that have been recorded erupting multiple times.

One can categorize novae into different speed classes based on their decline times, t_2 and t_3 (Payne-Gaposchkin 1957). These denote the time taken to decay by 2 or 3 mag (respectively) from maximum light. Zwicky (1936) first proposed a relationship between the decline time and the maximum absolute visual magnitude of a nova. Subsequently, Mclaughlin (1945) and Arp (1956) developed the 'maximum magnitude–rate of decline' relation (MMRD; see e.g. Downes & Duerbeck 2000). However, the MMRD suffers from a large scatter, and the relation has been diluted by the discovery of 'faint and fast' novae (Kasliwal et al. 2011; Shara et al. 2016) and short-cycle RNe ($P_{\rm rec} < 10$ yr; Darnley & Henze, in preparation).

Independent studies of Galactic novae using *Gaia* data release 2 (DR2; Gaia Collaboration 2018) parallaxes appear to show

★ E-mail: M.W.Healy@2017.ljmu.ac.uk (MWH); M.J.Darnley@ljmu.ac.uk (MJD)

contradictory results. Schaefer (2018) proposes that the MMRD is an unusable distance determination method and that it should no longer be employed. However, Selvelli & Gilmozzi (2019) show that the MMRD relationship is strengthened once *Gaia* distances are assumed. Although there is some overlap, these two studies use different samples of novae. Shara et al. (2017) used a large sample of M 87 novae to clearly demonstrate (see their fig. 1) the impact of 'faint and fast' novae on the MMRD distribution and therefore that the concept is inherently flawed.

Novae may be divided into two spectroscopic classes based on the prominent non-Balmer emission lines in their early-post-maximum spectra: either He/N or Fe II (Williams 1992, 1994). The contribution of novae from each class varies between different galaxies, possibly due to variations in the dominant stellar population and metallicity of a given host (Shafter 2013). Novae from younger (disc) populations have higher mean WD masses than those from older (bulge) populations. High-mass WDs create lower mass but higher velocity ejecta than their low-mass counterparts, and are believed to produce the He/N dominant spectra, with the lower mass WDs creating the Fe II class (Williams 2012; Shafter 2013).

The study of novae in extragalactic environments provides the only way to explore how the local environment (e.g. the metallicity and star formation rate) can affect the nova rate and characteristics of nova eruptions (Shara et al. 2016). The M 31 nova population is dominated by the Fe II class (82 per cent; Shafter et al. 2011). Yet 'bulgeless' galaxies show similar numbers of each class. For example, 5 of the 10 spectroscopically classified novae in M 33 are Fe II; the M 33 spectral type distribution differs from that of M 31 at the 98 per cent confidence level (Shafter et al. 2012, 2014). The fraction of Fe II novae in the LMC is also ∼50 per cent (Shafter 2013).

NGC 6822 is a dark matter dominated (Weldrake, de Blok & Walter 2003) dwarf irregular galaxy in the Local Group at a distance 476 ± 44 kpc (Rich et al. 2014). It provides a low-metallicity environment compared to the majority of Local Group novae: [Fe/H] ≈ −0.5 (see e.g. Larsen et al. 2018).

AT 2017fvz[1] (aka KAIT-17bm) is only the second nova to be discovered within NGC 6822 (see Section 4.1 for a discussion of the first nova). It was discovered on 2017 August 2.384 UT with an unfiltered magnitude of 17.6 at $\alpha = 19^{\rm h}45^{\rm m}1\overset{\rm s}{.}03, \delta = -14^{\circ}46'50\overset{''}{.}74$ (J2000; Hestenes, Zheng & Filippenko 2017) by the Katzman Automatic Imaging Telescope (KAIT; Filippenko et al. 2001) of the Lick Observatory Supernova Search (LOSS). This nova was also observed by the All-Sky Automated Survey for Supernovae (ASAS-SN; see Shappee et al. 2014) on August 3.190 and then with the Asteroid Terrestrial-impact Last Alert System (ATLAS; Heinze et al. 2018; Tonry et al. 2018) on August 3.386.

Here we report optical, near-ultraviolet (NUV), and X-ray observations of the eruption of AT 2017fvz. In Section 2 we describe the observations and data analysis. In Section 3 we present the results of the photometry, spectroscopy, and X-ray analysis, and we discuss these in Section 4. We summarize our findings in Section 5. Throughout, all times are quoted in coordinated universal time (UT), all uncertainties are quoted to 1σ, and all upper limits to 3σ.

[1] https://wis-tns.weizmann.ac.il/object/2017fvz.

2 OBSERVATIONS AND ANALYSIS

2.1 Ground-based photometry

The field containing the nova had been monitored by KAIT using its clear filter since 2017 July 15.404 without any associated detections until the discovery on August 2.384, after which the nova was followed until August 31.284. ATLAS monitored a similar field from July 5.477 using its 'orange' filter, approximately covering r' and i' (5600–8200 Å),[2] without any associated detections until the first detection on August 3.386. Like KAIT, the nova was monitored after discovery by ATLAS for the next 47 d until September 19.317 using the orange filter and also a 'cyan' filter which approximately covers V and r' (4200–6500 Å). A few hours before the ATLAS detection, the nova was detected by ASAS-SN on 2017 August 3.190 with a V-band filter. A Liverpool Telescope (LT; Steele et al. 2004) follow-up campaign began 7.53 d post-discovery; observations were taken with IO:O[3] through $u'BVr'i'$ filters.

Debiasing and flat-fielding of the LT data were performed by the automatic LT reduction pipeline. Aperture photometry was calculated from these data using standard tools within PYRAF and calibrated against stars from the Local Group Galaxies Survey (LGGS; Massey et al. 2007). The $u'r'i'$ magnitudes of the LGGS stars were calculated using transformations from Jester et al. (2005, their table 1). Each time spectra were obtained with the SPectrograph for the Rapid Acquisition of Transients (SPRAT; Piascik et al. 2014, see Section 2.2) by the LT, acquisition images were also taken using the SPRAT detector. These images were reduced in the same manner as the IO:O data. The acquisition images were unfiltered, but the photometry was calibrated relative to the r' filter.

The KAIT data were reduced using a custom pipeline (Ganeshalingam et al. 2010). Point spread function (PSF) photometry was obtained using the IDL implementation of DAOPHOT (Stetson 1987; Landsman 1993). Several nearby stars from the APASS catalogue (Henden et al. 2009) were used to calibrate the KAIT clear-band data, with their magnitudes converted to the Landolt R-band system using the empirical prescription presented by R. Lupton.[4]

ATLAS carries out difference imaging of every frame with respect to a reference sky and the photometry reported here is from those images. The photometry was carried out as described by Tonry et al. (2018) and Stalder et al. (2017).

2.2 Spectroscopy

The optical spectra of AT 2017fvz were taken using SPRAT on the LT. SPRAT is a spectrograph with a slit 95 arcsec long and 1.″8 wide giving a resolution of 18 Å per pixel, corresponding to $R \approx 350$ at the centre of the spectrum. It covers visible wavelengths in the range 4000–8000 Å. The details of the spectra, which were obtained using the blue-optimized mode, are summarized in Table 1. All spectra were extracted, wavelength calibrated, and flux calibrated using the SPRAT pipeline (Piascik et al. 2014), except for the August 25 spectrum which was not flux calibrated owing to poor sky transparency (clouds). The spectra were then analysed using routines with PYRAF.

[2] http://www.fallingstar.com/specifications.php.
[3] http://telescope.livjm.ac.uk/TelInst/Inst/IOO.
[4] http://sdss.org/dr7/algorithms/sdssUBVRITransform.html.

Table 1. LT SPRAT spectroscopy of AT 2017fvz.

UT Date[a]	MJD (d)	$t - t_0$ (d)	Exposure time (s)
2017-08-09.900	57974.900	8.016	3 × 600
2017-08-15.924	57980.924	14.040	3 × 600
2017-08-19.894	57984.894	18.010	3 × 600
2017-08-25.885	57990.885	24.001	3 × 600
2017-09-12.879	58008.879	41.995	3 × 900
2017-10-10.848	58036.848	69.964	3 × 900

[a]The date refers to the mid-point of each observation.

2.3 *Swift* NUV and X-ray observations

Five target-of-opportunity (ToO) observations with the Neil Gehrels *Swift* Observatory (Gehrels et al. 2004), totalling 20.0 ks, were utilized to follow the NUV and X-ray evolution of the AT 2017fvz (Target ID: 10268). We summarize all of the *Swift* data in Table 2.

NUV data were obtained with the UV/Optical Telescope (UVOT; Roming et al. 2005) through the *uvw1* filter. X-ray data were collected by the X-ray Telescope (XRT; Burrows et al. 2005) in photon-counting mode. The NUV data were processed with HEASOFT tools (v6.24; Blackburn 1995) and using the most recent calibration files. We extracted the count-rate upper limits from the X-ray data using the online *Swift* XRT tool[5] (Evans et al. 2009).

3 RESULTS

3.1 Reddening

NGC 6822 has a Galactic longitude and latitude of $\ell = 25.4^\circ$ and $b = -18.4^\circ$, respectively (Mateo 1998). This results in that galaxy being affected by a modest amount of foreground Milky Way extinction. Kayser (1967) found the Galactic reddening towards the outer regions of NGC 6822 to be $E_{B-V} = 0.27 \pm 0.03$ mag, as did Massey et al. (1995) with $E_{B-V} = 0.26$ mag. These are consistent with Gallart, Aparicio & Vilchez (1996) and Massey et al. (2007) who found $E_{B-V} = 0.24 \pm 0.03$ mag and $E_{B-V} = 0.25$ mag, respectively. The online dust-mapping tool[6] (Green et al. 2018) returns a Galactic reddening towards NGC 6822 of $E_{B-V} = 0.22 \pm 0.02$ mag.

Cepheid variables within NGC 6822 have been employed to estimate the internal reddening. McAlary et al. (1983) found $E_{B-V} = 0.36$ mag, Gieren et al. (2006) reported a similar average reddening of $E_{B-V} = 0.36 \pm 0.01$ mag. Rich et al. (2014) used optical and infrared data for Cepheids to determine that the foreground reddening along the line of sight to NGC 6822 is $E_{B-V} = 0.35 \pm 0.04$ mag.

We have no knowledge of the radial displacement of AT 2017fvz within NGC 6822 so we adopt the two most extreme values of reddening. The foreground reddening towards NGC 6822 gives the lower limit, the addition of reddening internal to NGC 6822 gives the upper limit.

3.2 Photometric evolution

The AT 2017fvz photometry from ASAS-SN, ATLAS, KAIT, LT, and *Swift* are presented in Fig. 1 and in Tables A1–A3. The light curves illustrate that the nova was discovered prior to peak optical magnitude. We calculate the time of eruption to be 2017 August 1.9 ± 0.5, the mid-point between the last non-detection (KAIT) with $m_{\rm clear} > 18.1$ mag on 2017 August 1.384 and the discovery on August 2.384. Throughout, we refer to the time of eruption as t_0.

The u', B, and V bands all fade at approximately the same rate from peak until around 40 d, while i' fades more slowly and r' even slower owing to the strong influence of the Hα emission line on the broad-band photometry. We estimated the decline times (t_2 and t_3) of AT 2017fvz by taking the brightest data point as the peak of the eruption and assuming a power-law decline (in luminosity; see e.g. Hachisu & Kato 2006). The decline times for each filter are recorded in Table 3. If we utilize the decline times with the MMRD relation (Downes & Duerbeck 2000), then we would expect peak absolute magnitudes of $M_V = -9.0 \pm 0.5$ and $M_V = -9.0 \pm 0.7$ for t_2 and t_3, respectively. It should be noted that this MMRD was derived from Galactic novae and, in addition to other limitations, may not be reliable within the differing environment of NGC 6822 (see Section 4.3).

Taking the distance modulus of NGC 6822 as $\mu_0 = 23.38 \pm 0.02$ mag (Rich et al. 2014), correcting for foreground reddening using $E_{B-V} = 0.22 \pm 0.02$ mag, we derive a lower limit for the peak absolute magnitude of $M_V = -7.41 \pm 0.07$. Here, we assumed that the peak observed magnitude (ASAS-SN) corresponded to the peak of the eruption. By extrapolating the V-band light curve power-law fit back to the final pre-eruption non-detection, we can estimate an upper limit on the peak eruption magnitude. Combining this upper limit with the estimate of the total (foreground and internal) reddening ($E_{B-V} = 0.36 \pm 0.01$ mag) yields an upper limit for the peak absolute magnitude of $M_V = -8.33 \pm 0.05$.

There is evidence for a 'plateau' in the u-, B-, V-, and i'-band light curves around $t = 25$ d. As such, this nova would belong to the 'plateau' class (P-class; Strope, Schaefer & Henden 2010), where an otherwise smoothly declining light curve is interrupted by a short period when the optical magnitude remains approximately constant.

3.3 Spectroscopic evolution

To aid the analysis of the AT 2017fvz spectra, we made extensive use of spectral line data from Moore (1945) and Williams (2012). All of the spectra of AT 2017fvz are plotted in Fig. 2. These spectra can be split into three groups: the first contains the first four spectra that are within a ∼16 d-long period during early decline; the fifth spectrum was taken at $t \approx 42$ d during the plateau, and the sixth was taken at $t \approx 70$ d during the nebular phase. The spectra are presented in the rest frame of the observer. The average radial velocity of NGC 6822 is -57 km s^{-1} (Koribalski et al. 2004). The flux and full width at half-maximum intensity (FWHM) velocity were calculated by fitting Gaussian profiles to the emission lines using the SPLAT package in STARLINK; the fluxes and velocities are reported in Tables 4 and 5, respectively.

3.3.1 Early decline

The first spectrum was taken at $t = 8.016$ d when the nova was in the early decline phase (Williams & Darnley 2017). By this time, we have missed the optically thick 'fireball' stage which occurs on the rise until around peak brightness. We may have caught the very end of this transition with some of the Fe II lines and the Hδ emission line still showing tentative signs of P Cygni profiles. The Hδ line has a small blueshifted absorption component with a mid-point of

[5]http://www.swift.ac.uk/user_objects/.
[6]http://argonaut.skymaps.info.

Table 2. *Swift* UVOT photometry and XRT counts for AT 2017fvz.

Exp[a] (ks)	Date[b] (UT)	MJD (d)	$t - t_0^c$ (d)	*uvw*1[d] (mag)	X-ray rate (10^{-3} ct s^{-1}) 0.3–1 keV	0.3–10 keV	L^e (10^{37} erg s^{-1}) 0.3–1 keV	0.3–10 keV
3.9	2017-09-09	58005	38.12	18.6 ± 0.1	<1.9	<1.9	<0.8	<0.8
3.7	2017-10-08	58034	67.12	19.4 ± 0.2	<3.5	<3.3	<1.4	<1.3
3.4	2017-11-07	58064	97.12	19.6 ± 0.3	<2.5	<3.2	<1.0	<1.3
3.7	2018-04-27	58235	268.12	20.2 ± 0.3	<3.4	<3.2	<1.3	<1.3
4.0	2018-08-25	58355	388.12	19.9 ± 0.2	<2.5	<3.0	<1.0	<1.2

[a]Dead-time corrected XRT exposure time.
[b]Start date of the observation.
[c]Time since day of eruption on 2017 Aug. 1.884.
[d]Vega magnitudes for the *uvw*1 filter (central wavelength: 2600 Å).
[e]X-ray luminosity upper limits (unabsorbed, blackbody fit, 0.3–1 keV or 0.3–10 keV, as indicated).

4052 ± 8 Å and an equivalent width of 29 ± 6 Å. Also, the emission component may have a different profile than the other Balmer lines with an FWHM of ∼2400 km s^{-1}. In Fig. 3 we show the Balmer lines from the first three spectra to illustrate the tentative evidence for an H δ P Cygni profile.

As the predominant non-Balmer emission lines are those of iron, AT 2017fvz is consistent with the Fe II class. The broad Balmer lines lie close to the border value of 2500 km s^{-1} which defines the broad-lined Fe II novae class (Fe IIb; Shafter et al. 2009).

The other prominent features of this first spectrum are the H α, H β, and H γ emission lines and the double-peaked O I (1) emission line at 7773 Å, all of which have FWHM velocities of ∼2400 km s^{-1}. There is an Fe II (42) triplet redward of H β at 4924, 5018, and 5169 Å, as well as a fairly strong Na I D emission line at ∼5892 Å. There may be a weak Fe II (74) multiplet blueward of H α with 6148 and 6456 Å lines visible. However, with the 6248 and 6417 Å lines clearly absent, the feature at 6456 Å is more likely to be associated with nitrogen. Another explanation for this line at 6148 Å could be O I λ6158. Between these lines, there is a feature at around 6300 Å, which is almost certainly [O I], that persists until the 'plateau' phase. We also see tentative evidence for Fe II (37) lines at 4556 and 4629 Å.

The second AT 2017fvz spectrum, taken 14.040 d post-eruption, maintains all aforementioned emission lines including the H I lines, which show slightly lower FWHM velocities of ∼2100 km s^{-1}, and many Fe II lines. In addition, a prominent feature has developed at around 4640 Å which may be a blend of N III and O II emission lines at 4638 and 4676 Å, respectively (see Section 3.3.2). Other emission lines could be present at this location including C IV λ4658, [Fe III] λ4658, or O I (18) at 4655 Å. The [O I] λ5577 line can be seen alongside the N II (3) line at 5679 Å, similar to V1494 Aquilæ (Nova Aql 1999) ∼14 d post-maximum (see fig. 6 in Iijima & Esenoglu 2003) and to SN 2010U,[7] 15.3 d post-maximum (see fig. 11 in Czekala et al. 2013).

The third spectrum ($t = 18.010$ d) is similar to the previous two, with all lines except H α (see Section 3.3.4), H β, and the blend at ∼4640 Å having weakened. Unfortunately, the fourth spectrum ($t = 24.001$ d) has low-signal-to-noise ratio owing to poor observing conditions, and only Balmer and [O I] λ6300 lines are apparent.

3.3.2 'Plateau' phase

The fifth spectrum was taken 41.995 d post-eruption during the apparent plateau phase. The H I emission lines still dominate, but these are joined by nitrogen emission lines such as N II (24) at 5001 Å, N II (3) at 5679 Å, and [N II] λ5755. During this evolutionary phase, we might expect to see a considerable enhancement of nitrogen lines – the so-called 'nitrogen flaring' – caused by the Bowen fluorescence mechanism whereby N III is 'pumped' by the UV resonance lines of O III (Bowen 1934, 1935). Harvey et al. (2018) suggested that this 'Bowen Blend' (∼4640 Å) may be more naturally explained by 'oxygen flaring,' whereby there is flaring of the O II multiplet (V1) in the range 4638–4696 Å.

Such N- or O-flaring may manifest in the spectrum of AT 2017fvz through a broad amalgamation of lines at approximately 4640 Å, where it is difficult to distinguish the individual lines owing to the low spectral resolution. We assume that they are the N II (5) multiplet at 4614, 4621, and 4630 Å, and the C III (1) multiplet at 4647, 4650, and 4651 Å, as well as other nitrogen species.

3.3.3 Nebular phase

The final spectrum was taken 69.964 d post-eruption. Here, there is evidence for the [O III] nebular lines at 4959 and 5007 Å. Only a handful of novae beyond the Magellanic Clouds have been observed spectroscopically during this phase (Williams, Darnley & Henze 2017). The appearance of [O III] often roughly coincides with the beginning of the SSS phase when the ejecta from the nova are becoming optically thin to UV radiation and collisions are still occurring owing to the sufficiently high density providing a cooling mechanism (Mason et al. 2018). Additionally, the 'Bowen Blend' is still visible but has broadened and taken on a 'dome-like' appearance.

At this time, the density of the ejecta must be less than the critical density ($n_e^{\rm crit} = 6.8 \times 10^5$ cm^{-3}) for the collisional de-excitation of [O III]. One might also expect the [O III] auroral line at 4363 Å; however, as this is a relatively weak line, it is most likely blended with H γ or hidden by the Hg I night-sky line at 4358 Å. Even so, we can use the ratio of these three emission lines to estimate an upper limit for the electron temperature within this part of the ejecta of 5000 K (see fig. 5.1 in Osterbrock & Ferland 2006).

3.3.4 H α evolution

The evolution of the H α emission-line profile is shown in Fig. 4. After the first spectrum at $t \approx 8$ d, when the line has an FWHM of 2430 ± 70 km s^{-1}, the line progressively narrows from 2300 ± 100 km s^{-1} to 2070 ± 70 km s^{-1} and then 2000 ± 90 km s^{-1} at $t \approx 14$ d, $t \approx 18$ d, and $t \approx 24$ d, respectively. The line width then remains constant between the fifth and sixth spectra with the FWHM

[7]Not a supernova (Czekala et al. 2013).

Table 3. Decline times of AT 2017fvz in each filter.

Filter	t_2 (d)	t_3 (d)
u'	7.1 ± 0.2	13.7 ± 0.3
B	7.0 ± 0.2	13.3 ± 0.3
V	8.1 ± 0.2	15.2 ± 0.3
r'	15.5 ± 0.4	33 ± 1
i'	13.0 ± 0.3	25.3 ± 0.6

being $1840 \pm 60\,\mathrm{km\,s^{-1}}$ at $t \approx 42$ d and $1900 \pm 100\,\mathrm{km\,s^{-1}}$ at $t \approx 70$ d. With no evidence for substantial circumbinary material, such line narrowing is probably due to decreasing emissivity as the ejecta expand, rather than a deceleration.

3.4 X-rays

Utilizing the r'-band decline time ($t_2 \approx 15$ d; see Table 3), we used the correlations presented by Henze et al. (2014) to predict the expected SSS properties of AT 2017fvz. These indicate that an SSS

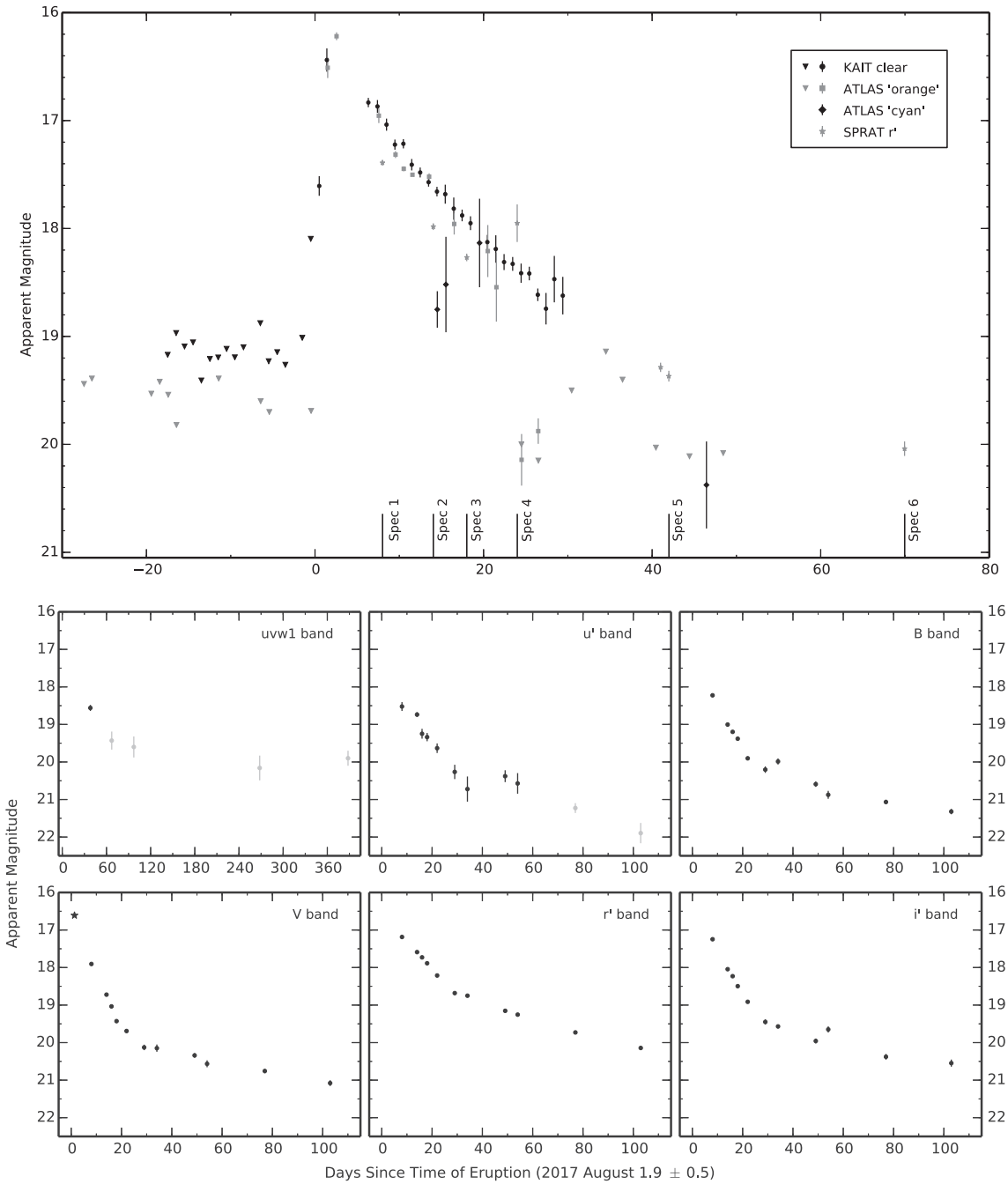

Figure 1. Multiband light curves of AT 2017fvz. Top: Optical light curve; see key for data sources. The epochs of the SPRAT spectra are indicated along the bottom axis. Lower panels: Light curves through individual filters. The star close to peak brightness in the *V*-band plot is from ASAS-SN. The grey points in the *uvw1* and *u'* panels are possibly contaminated by a nearby unresolved source (see Section 3.5). Note that the *uvw1* plot covers ∼420 d.

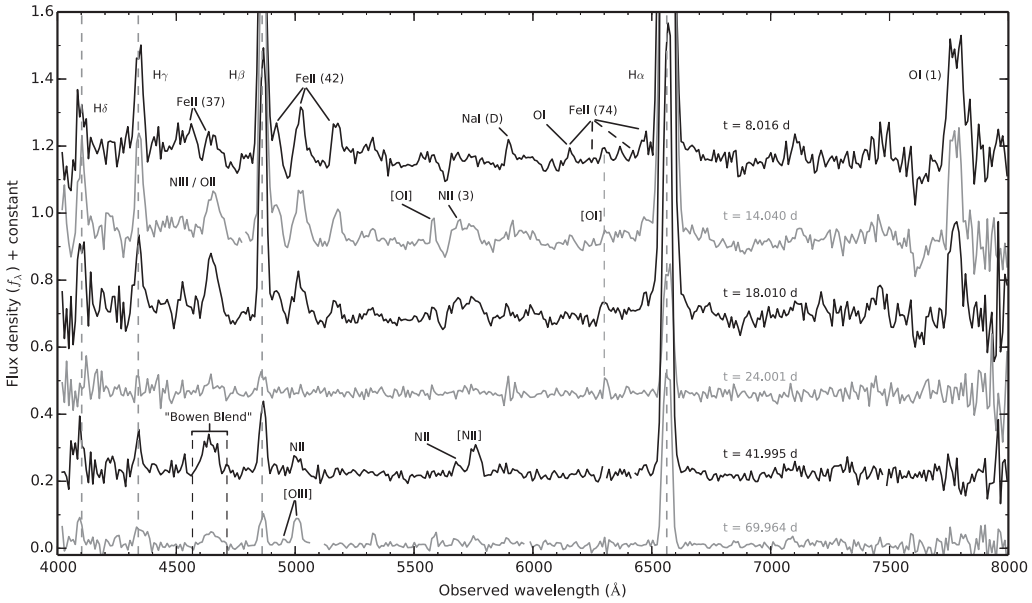

Figure 2. The six SPRAT spectra of AT 2017fvz, where the times post-eruption for each spectrum and prominent emission lines are indicated with labels. The gaps in the spectra at $t = 14.040$ d, $t = 41.995$ d, and $t = 69.964$ d were the locations of substantial cosmic rays.

Table 4. The evolution of emission-line fluxes from the spectra of AT 2017fvz in units of 10^{-15} erg cm^{-2} s^{-1}.

Line identification rest wavelength (Å)	$t = 8.016$ d	$t = 14.040$ d	$t = 18.010$ d	$t = 41.995$ d	$t = 69.964$ d
H δ (4102)	6 ± 3	8 ± 2	7 ± 3	2 ± 1	1.7 ± 0.4
H γ (4341)	12 ± 1	9 ± 1	7 ± 1	2.4 ± 0.5	2.0 ± 0.6
H β (4861)	30 ± 3	31 ± 4	27 ± 2	6.8 ± 0.5	2.4 ± 0.5
[O III] (5007)	–	–	–	–	2.6 ± 0.4
Fe II (5018)	4.6 ± 0.7	5 ± 1	–	–	–
H α (6563)	139 ± 6	210 ± 10	230 ± 10	61 ± 3	24 ± 2
O I (7773)	28 ± 4	22 ± 3	16 ± 2	–	–

We have not included the spectrum from 24.001 d after eruption because the fluxes are not reliable.

Table 5. The evolution of emission-line velocities from the spectra of AT 2017fvz in units of km s^{-1}.

Line identification rest wavelength (Å)	$t = 8.016$ d	$t = 14.040$ d	$t = 18.010$ d	$t = 24.001$ d	$t = 41.995$ d	$t = 69.964$ d
H δ (4102)	2600 ± 900	2100 ± 300	2100 ± 600	–	900 ± 50	1500 ± 300
H γ (4341)	2500 ± 200	2000 ± 200	2200 ± 300	–	1400 ± 200	3500 ± 800 [a]
H β (4861)	2300 ± 200	2100 ± 200	1900 ± 100	–	1800 ± 100	1600 ± 200
[O III] (5007)	–	–	–	–	–	1900 ± 200
Fe II (5018)	1900 ± 200	2200 ± 200	–	–	–	–
H α (6563)	2430 ± 70	2300 ± 100	2070 ± 70	2000 ± 90	1840 ± 60	1900 ± 100
O I (7773)	2800 ± 300	2200 ± 200	2000 ± 200	–	–	–

[a]This velocity is an upper limit as the H γ line is blended with other lines around this wavelength.

with blackbody temperature $kT \approx 50$ eV should have appeared at $t_{on} \approx 72$ d and turned off at $t_{off} \approx 243$ d.

A Galactic foreground column density of $N_H = 10^{21}$ cm^{-2} towards AT 2017fvz was derived from the HEASARC N_H tool based on the Galactic neutral hydrogen map by Kalberla et al. (2005). We used the PIMMS software (v4.8f) with this column and the estimated SSS temperature to convert from counts to unabsorbed flux. We then derived X-ray luminosities by assuming a distance of 476 kpc to NGC 6822; these are presented in Table 2.

We do not detect any X-ray emission from AT 2017fvz in any of the five visits between 38 and 388 d post-eruption. The luminosity upper limits, calculated from the X-ray count limits (0.3–1 keV), assuming $kT \approx 50$ eV in Table 2, are all below 1.4×10^{37} erg s^{-1}. The assumed temperature is low compared in particular to fast RNe such as M31N 2008-12a (∼120 eV; Darnley et al. 2016) and RS Oph (∼90 eV; Osborne et al. 2011); therefore, AT 2017fvz must not have had a bright SSS phase during our observational window.

3.5 The nova progenitor

A nova system may harbour either a main-sequence, subgiant, or red giant donor. If AT 2017fvz hosted a red giant or a luminous accretion

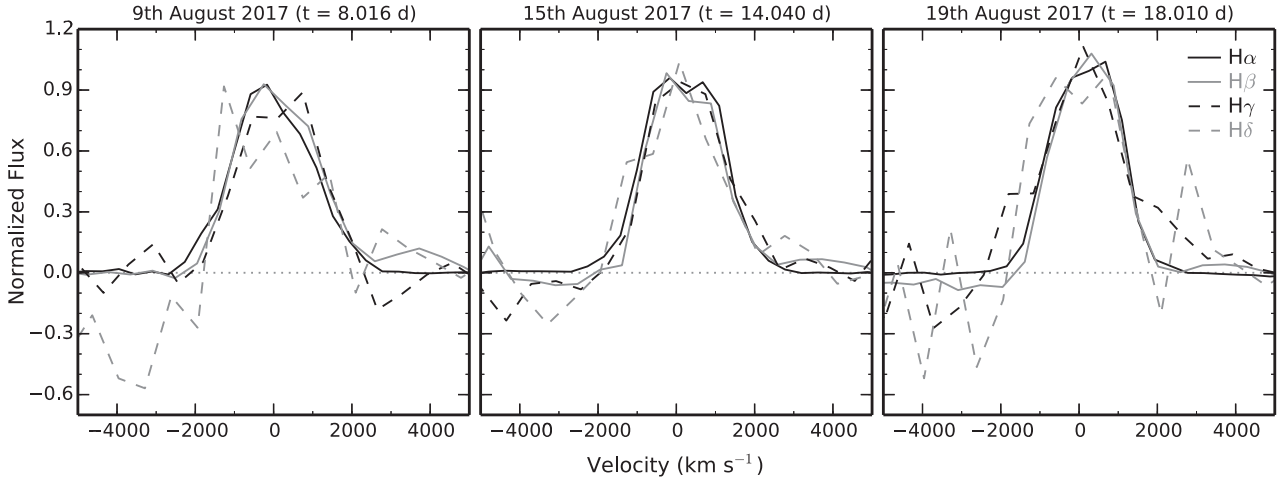

Figure 3. The evolution of the AT 2017fvz H α–H δ emission lines over ∼18 d post-eruption (normalized to peak flux). The H δ profile shows tentative evidence for blueshifted absorption ($t = 8.016$ d) – a possible P Cygni profile.

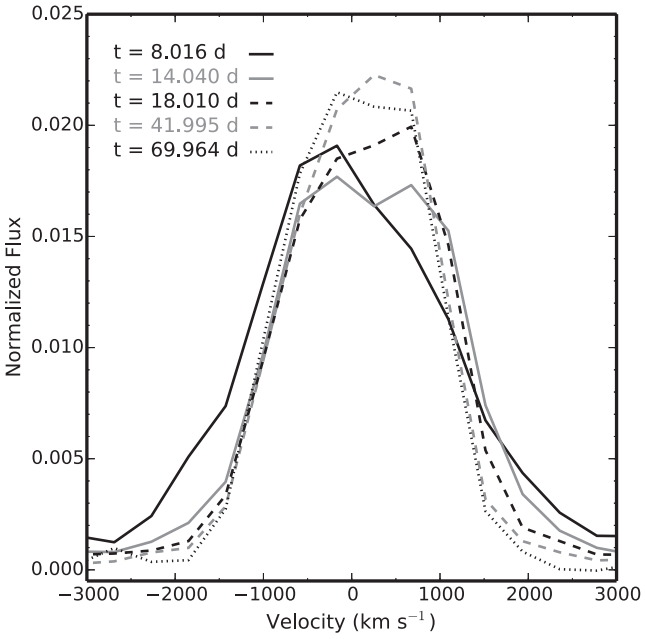

Figure 4. H α emission-line evolution from $t = 8$ d to $t = 70$ d in terms of normalized flux and velocity. The $t = 24$ d spectrum is not included owing to lack of flux calibration.

disc then it could have been detectable with *Hubble Space Telescope* (*HST*) owing to the proximity of NGC 6822 (Williams et al. 2014). AT 2017fvz is located within archival *HST* Wide-Field Planetary Camera 2 (WFPC2) images (GO-11079) taken through the F170W, F255W, F336W, F439W, F555W, and F814W filters.

As described by Bode et al. (2009), Darnley et al. (2014), and in detail by Williams et al. (2014), we used reference stars in the LT images and an F814W *HST* image to compute a precise astrometric transformation between the data sets. We extended the technique by employing all 18 of the i'-band and r'-band LT images of AT 2017fvz to calculate the average nova position (and subsequent scatter) to more precisely and accurately constrain the nova position in the *HST* data, as shown in Fig. 5.

We performed crowded-field PSF fitting photometry with DOLPHOT (v2.0; Dolphin 2000, using standard WFPC2 parameters) on all detected objects in the *HST* image, recovering a source that is within 5.14σ (2.05 WFPC2/PC pixels) of AT 2017fvz, an angular separation of 0.″0931, or a projected distance of 0.21 pc (see Fig. 5 for the position and Table 6 for the photometry of the source). While seemingly close, we have no knowledge of the line-of-sight separation of the two objects. A colour–magnitude diagram based on these *HST* data was used to determine a limiting magnitude of $m_{\rm F814W} \approx 23.5$. Using the method described by Williams et al. (2016), the probability of a coincidental alignment between AT 2017fvz and this source is 18 per cent. This does not meet the criterion (≤5 per cent) employed by Williams et al. (2016) to confirm a likely nova candidate. The astrometric separation indicates with high confidence that this is indeed a chance alignment. The absence of a detected progenitor within the *HST* data indicates that the system is highly likely to harbour a main-sequence or subgiant donor, and that the mass accretion rate is modest at best.

The proximity of this bright source to the nova (∼0.″1) may have contaminated the ground-based and *Swift* photometry. Therefore, we determined this source's luminosity in the F814W, F555W, F336W, and F170W filters. Its spectral energy distribution (SED) is shown in Fig. 6 and compared to the SED evolution of AT 2017fvz. The source is extremely bright in the NUV, indicating that it is most likely to be an O or B star. The AT 2017fvz SEDs clearly illustrate the influence that the H α emission of the nova has on the r'-band photometry. The final AT 2017fvz u'-band observation (∼103 d post-eruption) is consistent with the *HST* F336W photometry (similar wavelengths), indicating that the late-time u' photometry is contaminated by this nearby source. The *Swift* photometry is similarly adversely affected.

A fit to the SED (*HST* plus *Swift* data) of the nearby source is consistent with the Rayleigh–Jeans tail of a blackbody with $T_{\rm eff} = 40000 \pm 8000$ K and $M \approx -10.1$ mag ($\chi^2_{\rm red} = 1.68$), at the distance of NGC 6822 and assuming $E_{B-V} = 0.22$ mag. Such a temperature and luminosity are consistent with an O star. However, the F814W photometry is significantly brighter than would be expected for such a star.

4 DISCUSSION

4.1 The previous nova in NGC 6822

There has only been one previous observed nova in NGC 6822, which was discovered independently by King & Li (1999) and

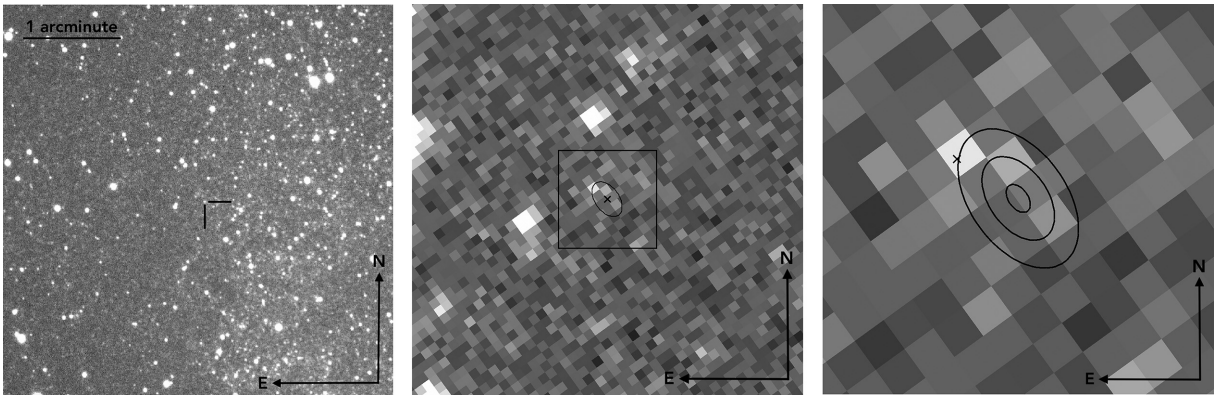

Figure 5. The location of AT 2017fvz. Left: A 4×4 arcmin^2 subset of an LT *V*-band image of AT 2017fvz taken 49 d post-eruption. The position of AT 2017fvz is indicated by the two black lines. Middle: A 2×2 arcsec^2 subset of the *HST* WFPC2 F814W image from April 2007 of the nova field. The black ellipse is the 5σ uncertainty in the position of the nova (black $\times$). The black box indicates the zoomed-in region in the right image. Right: $0\farcs5 \times 0\farcs5$ region around AT 2017fvz in the *HST* image. The black ellipses show the 1σ, 3σ, and 5σ uncertainties on the position of the nova. The black cross is a nearby source not resolvable from the ground.

Table 6. *HST*/WFPC2 photometry of the nearby source.[a]

Filter	Photometry (mag)
F170W	18.481 ± 0.480
F255W	–
F336W	20.982 ± 0.392
F439W	–
F555W	23.372 ± 0.201
F814W	22.259 ± 0.137

[a]No source was detected in the F255W or F439W data.

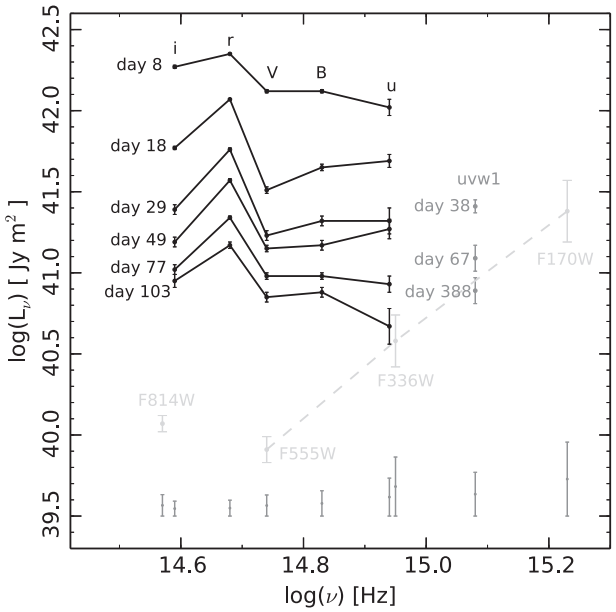

Figure 6. SED of AT 2017fvz (from 8 to 103 d post-eruption) and the source within $0\farcs1$. Black points are optical photometry of AT 2017fvz, grey points are from the *uvw*1 photometry. The light grey points are photometry associated with the nearby source, with one of the points being the apparently discrepant F814W photometry. The grey bars at the base are the combined systematic uncertainties from the distance and extinction toward NGC 6822.

Wei et al. (1999). That nova, located at $\alpha = 19^{\rm h}45^{\rm m}0\fs31$, $\delta = -14^\circ50'10\farcs3$ (J2000), was discovered by KAIT in unfiltered images taken on 1999 June 23.40 and 23.44 with $m \approx 17.3$ mag, and by the Beijing Astronomical Observatory Supernova Survey on June 23.69 and 24.72 with an unfiltered magnitude of 18. The nova was then imaged on June 24.38 by LOSS with an unfiltered apparent magnitude of ~17.0 and by the 1 m telescope at Sutherland Observatory on June 26.08 and 28.07 with *V*-band apparent magnitudes of 19.0 ± 0.1 and 19.6 ± 0.1, respectively (Bakos & PLANET Collaboration 1999).

This nova was spectroscopically confirmed on 1999 July 9 using the Kast spectrograph on the 3 m Shane telescope at Lick Observatory (Filippenko 1999). If we assume that the optical peak occurred at discovery, then this spectrum was taken on $t \approx 16$ d, roughly comparable to the $t \approx 14$ d and $t \approx 18$ d spectra of AT 2017fvz. This spectrum is published for the first time in Fig. 7 alongside a stacked spectrum of AT 2017fvz from $t \approx 8$ d, $t \approx 14$ d, and $t \approx 18$ d for comparative purposes.

Just as we see in the spectra of AT 2017fvz, there are prominent Balmer lines and many of the same Fe II lines. Blueward of H β there is Fe II (37) at 4629 and 4666 Å and redward there is Fe II (42) at 4924, 5018, and 5169 Å. The Fe II (74) multiplet is located to the blue of H α at 6148, 6248, 6417, and 6456 Å, and again O I λ6158 may contribute to the emission line at 6156 Å. The Na I D and [O I] emission lines at 5892 and 6300 Å (respectively) are also present and much more apparent. As well as the large number of Fe II lines between H β and H γ that were not clearly visible in the AT 2017fvz spectrum, we see the Fe II (49) multiplet at 5235, 5276, and 5326 Å to the red of the Fe II (42) multiplet. There is a feature in the spectrum at approximately 5533 Å which may also be Fe II and a feature at 5573 Å which is likely to be [O I] λ5577 given the prominence of the [O I] λ6300 emission line.

Many of the lines, such as Na I D, Fe II (42), and the Balmer lines have P Cygni profiles indicating that this spectrum was taken as the nova transitioned from the fireball stage. Comparing directly to the evolution of AT 2017fvz implies that the 1999 nova evolved more slowly, which is consistent with the much narrower emission lines. See Table 7 for the emission-line velocities of many of the prominent emission lines with the corresponding velocities for AT 2017fvz.

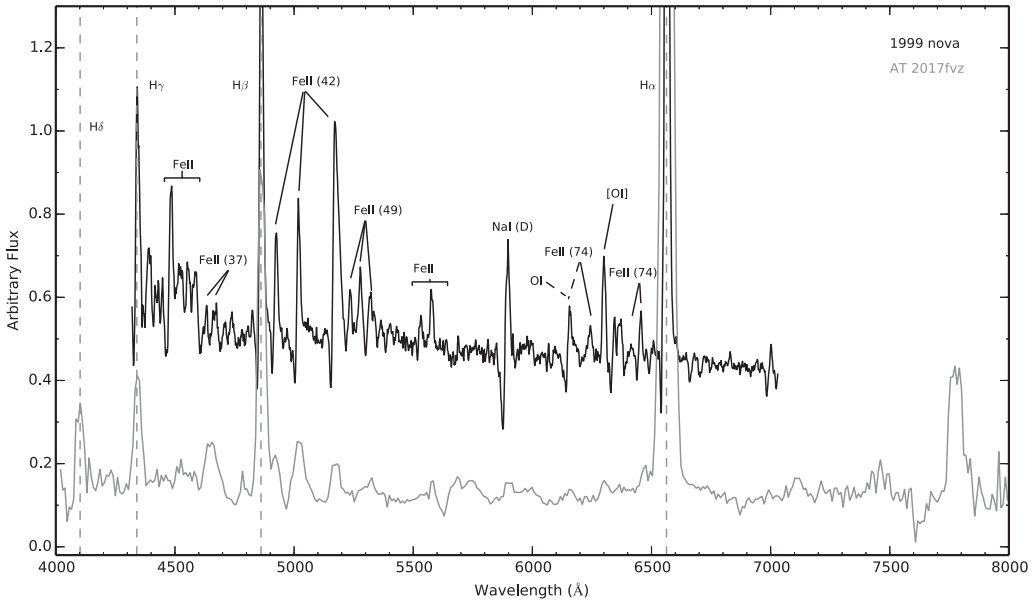

Figure 7. Stacked early-time AT 2017fvz spectrum ($t = 8$, 14, 18 d) compared to the spectrum of the 1999 nova taken on 1999 July 9 (∼16 d post-discovery).

Table 7. Comparison of emission-line FWHM velocities (km s^{-1}).

Line identification	Wavelength (Å)	1999 nova (NGC 6822)	AT 2017fvz ($t = 14.040$ d)
H γ	4341	900 ± 120	2000 ± 200
Fe II (37)	4491	910 ± 60	–
H β	4861	970 ± 50	2100 ± 210
Fe II (42)	4924	840 ± 50	–
Fe II (42)	5018	840 ± 80	2200 ± 230
Fe II (42)	5169	1500 ± 110	–
Fe II (49)	5235	860 ± 30	–
Fe II (49)	5276	1120 ± 50	–
Fe II (49)	5326	1600 ± 150	–
Fe II	5533	840 ± 90	–
[O I]	5577	850 ± 60	–
Na I D	5892	800 ± 130	–
[O I]	6300	650 ± 40	–
H α	6563	830 ± 20	2300 ± 100

4.2 The lack of X-rays

We do not detect X-ray emission from AT 2017fvz in any of the five *Swift* observations. This presents two scenarios: either the emission was not detectable, or it was detectable but we did not observe the system at the correct time.

There are two reasons why the X-rays emanating from the WD surface may not have been detectable. One option is that the X-ray emission may have ceased before the ejecta surrounding the nova were sufficiently diffuse to permit observation – that is, $t_{\rm off} < t_{\rm on}$.

The alternative is that the SSS may have been too faint to be detected, below the X-ray luminosity upper limit of $\sim 10^{37}$ erg s^{-1}. A number of SSSs in M 31 have been particularly faint, but these have been limited to (suspected) slow novae. M31N 2003-08c had a luminosity of 3.5×10^{36} erg s^{-1} when it was first detected ∼1540 d post-eruption and M31N 2006-09c had a luminosity $\leq 4.0 \times 10^{36}$ erg s^{-1} ∼426 d post-eruption (Henze et al. 2011). Both lacked photometric data to compute decline times, but we can reasonably assume that they are slow novae owing to their low ejecta velocities. The FWHM of the H α emission line in M31N 2003-08c is 900 km s^{-1} (di Mille et al. 2003) and M31N 2006-09c has an expansion velocity of 570 ± 45 km s^{-1} (Henze et al. 2011). Given their low ejection velocities, the observed turn-on times for these novae are fairly consistent with estimates determined from Henze et al. (2014) for $t_{\rm on}$. As such, we would not expect such a late $t_{\rm on}$ for AT 2017fvz. As AT 2017fvz does not belong to the slow speed class, a faint X-ray luminosity is potentially explained by the low-metallicity environment of NGC 6822. Depending upon the amount of mixing between the accreted envelope and the underlying WD, the metallicity of the accreted shell will either only weakly (strong mixing) or strongly (little mixing) depend upon the metallicity of the donor. As the TNR operates via the hot-CNO cycle, a lower metallicity shell might therefore be expected to produce a lower luminosity, but a longer lived SSS phase. In such a scenario, low metallicity alone might explain the lack of any X-ray detection. Orio (2013) provides further discussion about SSS populations within the SMC, a possibly similar environment to that of NGC 6822.

Alternatively, if the X-ray emission was in principle detectable, then the reasons for not observing this SSS phase revolve around the timing of the observations. It may also indicate that the Henze et al. (2014) correlations used to predict $t_{\rm on}$ and $t_{\rm off}$ (derived from CNe in M 31) are not valid in the lower metallicity environment of NGC 6822 (see e.g. Williams et al. 2017). First, the supersoft X-ray source may occur after 388 d (our last *Swift* observation), so we have simply observed too early, indicative of high-mass ejecta and also a low-mass WD. Secondly, the whole SSS phase may have taken place within one of the observing gaps, either between 38 and 67 d, between 67 and 97 d, between 97 and 268 d, or between 243 and 388 d. Though unlikely, there are examples of very short SSS phases in fast novae such as M31N 2007-12d, which had an extremely short SSS phase of <20 d (Henze et al. 2011). Finally, the most tantalizing option is that the entire SSS phase took place before our first *Swift* observation, 38 d post-eruption. This would imply low-mass ejecta and a high-mass WD, and potentially a RN.

4.3 A possibly 'faint and fast' or recurrent nova?

With $t_{2,V} = 8.1 \pm 0.2$ d, AT 2017fvz is a 'very fast' fading nova. We calculated from the MMRD relations of Downes & Duerbeck (2000) an expected peak V-band absolute magnitude of $M_V \approx -9$, but with a peak absolute magnitude in the range $-7.41 > M_V > -8.33$ mag AT 2017fvz may be substantially fainter than 'expected.' Given this range, and after accounting for expected differences between the V-band and g filters (see Shafter et al. 2009), AT 2017fvz would lie below the MMRD (broadly consistent with the position of M31N 2008-11a) as presented by Kasliwal et al. (2011, see their fig. 12), which plots six 'faint and fast' novae by their t_2 and their peak absolute g-band magnitude. Here we suggest caution, as the upper end of this range (high internal extinction contribution and missed light-curve peak) is marginally consistent with the MMRD. We also note that Kasliwal et al. (2011) employed the Balmer decrement to correct for extinction towards many of their M 31 novae; however, Case B recombination is not valid in the early stages of nova evolution (see Williams et al. 2017, for a discussion).

The 'faint and fast' region of the MMRD phase space is populated by a number of Galactic (see fig. 13 in Kasliwal et al. 2011) and M 31 RNe. Pagnotta & Schaefer (2014) defined a number of key indicators for an RN masquerading as a CN (i.e. only one observed eruption). AT 2017fvz satisfies some of these; for example the short t_2 implies the presence of a high-mass WD. The high ejecta velocities (for an Fe II nova) inferred from the H α emission line (2430 ± 70 km s^{-1}) further reinforce this suggestion.

Additionally, there is a plateau in the optical light curve from around day 25 to day 45. It has been proposed that such plateaus are produced by the SSS irradiating a reformed, or surviving, accretion disc and the donor. The subsequent reprocessed optical light then dominates the light emitted by the nova ejecta, temporarily halting the decline of the light curve (Hachisu et al. 2000; Evans et al. 2008; Darnley et al. 2016). This could indicate that the accretion disc survived the eruption, pointing to a high accretion rate and/or low ejected mass – a reasonable indicator of an RN. However, it does not provide strong evidence in isolation. Additionally, the spectrum obtained during the plateau shows no evidence for narrow (or any) He II lines, a key signature of a hot disc (as in seen during the plateau phase of known RNe; e.g. Henze et al. 2018).

The other criteria suggested by Pagnotta & Schaefer (2014) require either far superior spectroscopy or identification of the quiescent system. AT 2017fvz matches all of their RN indicators that we can reasonably test. The lack of a detected progenitor also indicates the absence of a luminous accretion disc, therefore at most only a modest accretion rate. Even if this system were an RN, it certainly would not be a short-cycle recurrent system.

5 SUMMARY AND CONCLUSIONS

In this paper we present observations and analysis of AT 2017fvz, the second nova observed in the Local Group dwarf irregular galaxy NGC 6822. We carried out detailed photometric and spectroscopic observations of the nova from its initial rise through to the nebular phase. We summarize as follows.

(1) AT 2017fvz was spectroscopically confirmed as an Fe II nova, but exhibited broader than typical emission lines.

(2) The light-curve evolution indicates that AT 2017fvz may belong to the P-class (plateau) novae, a proposed indication of a surviving or reformed accretion disc.

(3) As a 'very fast' nova with a decline time $t_{2(V)} \approx 8$ d, the MMRD predicted peak magnitude is $M_V \approx -9$. Yet we estimate the observed peak is in the range $-7.41 > M_V > -8.33$.

(4) The rapid decline and possible low luminosity suggest that AT 2017fvz may be a 'faint and fast' nova.

(5) No X-rays were detected between 38 and 388 d post-eruption, therefore the SSS must have occurred within the first ~40 d, been fully obscured by the ejecta, or simply been too faint to be detectable – a possible metallicity effect.

(6) The progenitor system was not recoverable from *HST* data, indicating a main-sequence or subgiant donor.

We have also included, for the first time, the sparse available data for the other confirmed nova in NGC 6822. Although currently limited in number, the study of novae across a range of galaxy types will permit systematic studies of how environment – particularly metallicity – can affect the properties of novae.

ACKNOWLEDGEMENTS

The authors would like to thank Mike Shara for his role in refereeing the manuscript, and all those that have contributed to the discussion about this object. MWH acknowledges a PhD studentship from the UK Science and Technology Facilities Council (STFC). MJD received funding from STFC. KLP received funding from the UK Space Agency. The work of AVF's group at UC Berkeley has been generously supported by the TABASGO Foundation, the Christopher R. Redlich Fund, and the Miller Institute for Basic Research in Science (UC Berkeley); additional funding was provided by NASA/*HST* grant AR-14295 from the Space Telescope Science Institute (STScI), which is operated by the Association of Universities for Research in Astronomy (AURA), Inc., under NASA contract NAS5-26555. We thank the staff of the various observatories at which data were obtained. This work made extensive use of the Liverpool Telescope, which is operated by LJMU on the island of La Palma in the Spanish Observatorio del Roque de los Muchachos of the Instituto de Astrofisica de Canarias with financial support from STFC. This work has made use of data from the Asteroid Terrestrial-impact Last Alert System (ATLAS) project. ATLAS is primarily funded to search for new near-Earth asteroids, through NASA grant NN12AR55G issued under the guidance of Lindley Johnson and Kelly Fast. A byproduct of this search is a collection of images and catalogues of the survey area. The ATLAS science products have been made possible through the contributions of the Institute for Astronomy, the University of Hawaii, the Queen's University Belfast, STScI, and Harvard University. Katzman Automatic Imaging Telescope (KAIT) and its ongoing operation were made possible by donations from Sun Microsystems, Inc., the Hewlett-Packard Company, AutoScope Corporation, Lick Observatory, the NSF, the University of California, the Sylvia & Jim Katzman Foundation, and the TABASGO Foundation. Research at Lick Observatory is partially supported by a generous gift from Google. This research has made use of the American Association of Variable Star Observers Photometric All-Sky Survey (APASS) data base, located at the AAVSO web site. Funding for APASS has been provided by the Robert Martin Ayers Sciences Fund. PYRAF is a product of STScI, which is operated by AURA for NASA.

REFERENCES

Arp H. C., 1956, AJ, 61, 15
Aydi E. et al., 2018, MNRAS, 474, 2679

Bakos G., PLANET Collaboration, 1999, IAU Circ., 7211, 3
Blackburn J. K., 1995, in Shaw R. A., Payne H. E., Hayes J. J. E., eds, ASP Conf. Ser., Vol. 77, Astronomical Data Analysis Software and Systems IV. Astron. Soc. Pac., San Francisco, p. 367
Bode M. F., 2010, Astron. Nachr., 331, 160
Bode M. F., Darnley M. J., Shafter A. W., Page K. L., Smirnova O., Anupama G. C., Hilton T., 2009, ApJ, 705, 1056
Bowen I. S., 1934, PASP, 46, 146
Bowen I. S., 1935, ApJ, 81, 1
Burrows D. N. et al., 2005, Space Sci. Rev., 120, 165
Czekala I. et al., 2013, ApJ, 765, 57
Darnley M. J., Ribeiro V. A. R. M., Bode M. F., Hounsell R. A., Williams R. P., 2012, ApJ, 746, 61
Darnley M. J., Williams S. C., Bode M. F., Henze M., Ness J.-U., Shafter A. W., Hornoch K., Votruba V., 2014, A&A, 563, L9
Darnley M. J. et al., 2016, ApJ, 833, 149
di Mille F., Ciroi S., Botte V., Boschetti C. S., 2003, IAU Circ., 8231, 4
Dolphin A. E., 2000, PASP, 112, 1383
Downes R. A., Duerbeck H. W., 2000, AJ, 120, 2007
Evans A., Bode M. F., O'Brien T. J., Darnley M. J., eds, 2008, ASP Conf. Ser., Vol. 401. RS Ophiuchi (2006) and the Recurrent Nova Phenomenon. Astron. Soc. Pac., San Francisco, p. 1
Evans P. A. et al., 2009, MNRAS, 397, 1177
Filippenko A. V., 1999, IAU Circ., 7220, 2
Filippenko A. V., Li W. D., Treffers R. R., Modjaz M., 2001, in Paczynski B., Chen W.-P., Lemme C., eds, ASP Conf. Ser., Vol. 246, IAU Colloq. 183: Small Telescope Astronomy on Global Scales. Astron. Soc. Pac., San Francisco, p. 121
Gaia Collaboration, 2018, A&A, 616, A1
Gallart C., Aparicio A., Vilchez J. M., 1996, AJ, 112, 1928
Ganeshalingam M. et al., 2010, ApJS, 190, 418
Gehrels N. et al., 2004, ApJ, 611, 1005
Gieren W., Pietrzyński G., Nalewajko K., Soszyński I., Bresolin F., Kudritzki R.-P., Minniti D., Romanowsky A., 2006, ApJ, 647, 1056
Green G. M. et al., 2018, MNRAS, 478, 651
Hachisu I., Kato M., 2006, ApJS, 167, 59
Hachisu I., Kato M., Kato T., Matsumoto K., 2000, ApJ, 528, L97
Harvey E. J., Redman M. P., Darnley M. J., Williams S. C., Berdyugin A., Piirola V. E., Fitzgerald K. P., O'Connor E. G. P., 2018, A&A, 611, A3
Heinze A. N. et al., 2018, AJ, 156, 241
Henden A. A., Welch D. L., Terrell D., Levine S. E., 2009, in American Astronomical Society Meeting Abstracts #214. p. 669
Henze M. et al., 2011, A&A, 533, A52
Henze M. et al., 2014, A&A, 563, A2
Henze M. et al., 2018, ApJ, 857, 68
Hestenes J. C., Zheng W., Filippenko A. V., 2017, Transient Name Server Discovery Report, p. 831
Iijima T., Esenoglu H. H., 2003, A&A, 404, 997
Jester S. et al., 2005, AJ, 130, 873
Kalberla P. M. W., Burton W. B., Hartmann D., Arnal E. M., Bajaja E., Morras R., Pöppel W. G. L., 2005, A&A, 440, 775
Kasliwal M. M., Cenko S. B., Kulkarni S. R., Ofek E. O., Quimby R., Rau A., 2011, ApJ, 735, 94
Kayser S. E., 1967, AJ, 72, 134
King J. Y., Li W. D., 1999, IAU Circ., 7208, 3
Koribalski B. S. et al., 2004, AJ, 128, 16
Landsman W. B., 1993, in Hanisch R. J., Brissenden R. J. V., Barnes J., eds, ASP Conf. Ser., Vol. 52. Astronomical Data Analysis Software and Systems II. Astron. Soc. Pac., San Francisco, p. 246
Larsen S. S., Brodie J. P., Wasserman A., Strader J., 2018, A&A, 613, A56
Mason E., Shore S. N., De Gennaro Aquino I., Izzo L., Page K., Schwarz G. J., 2018, ApJ, 853, 27
Massey P., Armandroff T. E., Pyke R., Patel K., Wilson C. D., 1995, AJ, 110, 2715
Massey P., Olsen K. A. G., Hodge P. W., Jacoby G. H., McNeill R. T., Smith R. C., Strong S. B., 2007, AJ, 133, 2393
Mateo M. L., 1998, ARA&A, 36, 435
McAlary C. W., Madore B. F., McGonegal R., McLaren R. A., Welch D. L., 1983, ApJ, 273, 539
Mclaughlin D. B., 1945, PASP, 57, 69
Moore C. E., 1945, Contributions from the Princeton University Observatory, vol. 21. Princeton University, Princeton, New Jersey, p. 1
Orio M., 2013, Astron. Rev., 8, 71
Osborne J. P. et al., 2011, ApJ, 727, 124
Osterbrock D. E., Ferland G. J., 2006, Astrophysics of gaseous nebulae and active galactic nuclei. University Science Books, CA
Pagnotta A., Schaefer B. E., 2014, ApJ, 788, 164
Payne-Gaposchkin C., 1957, The Galactic Novae. North-Holland Pub. Co, Amsterdam
Piascik A. S., Steele I. A., Bates S. D., Mottram C. J., Smith R. J., Barnsley R. M., Bolton B., 2014, in Ramsay S. K., McLean I. S., Takami H., eds, Proc. SPIE Conf. Ser., Vol. 9147. Ground-based and Airborne Instrumentation for Astronomy V. SPIE, Bellingham, p. 91478H
Rich J. A., Persson S. E., Freedman W. L., Madore B. F., Monson A. J., Scowcroft V., Seibert M., 2014, ApJ, 794, 107
Roming P. W. A. et al., 2005, Space Sci. Rev., 120, 95
Schaefer B. E., 2018, MNRAS, 481, 3033
Selvelli P., Gilmozzi R., 2019, A&A, 622, A186
Shafter A. W., 2013, AJ, 145, 117
Shafter A. W., Rau A., Quimby R. M., Kasliwal M. M., Bode M. F., Darnley M. J., Misselt K. A., 2009, ApJ, 690, 1148
Shafter A. W. et al., 2011, ApJ, 734, 12
Shafter A. W., Darnley M. J., Bode M. F., Ciardullo R., 2012, ApJ, 752, 156
Shafter A. W., Curtin C., Pritchet C. J., Bode M. F., Darnley M. J., 2014, in Woudt P. A., Ribeiro V. A. R. M., eds, ASP Conf. Ser., Vol. 490. Stellar Novae: Past and Future Decades. Astron. Soc. Pac., San Francisco, p. 77
Shappee B. J. et al., 2014, ApJ, 788, 48
Shara M. M. et al., 2016, ApJS, 227, 1
Shara M. M. et al., 2017, ApJ, 839, 109
Stalder B. et al., 2017, ApJ, 850, 149
Starrfield S., Sparks W. M., Truran J. W., 1976, in Eggleton P., Mitton S., Whelan J., eds, Proc. IAU Symp., Vol. 73. Structure and Evolution of Close Binary Systems. Kluwer, Dordrecht, p. 155
Steele I. A. et al., 2004, in Oschmann J. M., Jr, ed., Proc. SPIE Conf. Ser., Vol. 548. Ground-based Telescopes. SPIE, Bellingham, p. 679
Stetson P. B., 1987, PASP, 99, 191
Strope R. J., Schaefer B. E., Henden A. A., 2010, AJ, 140, 34
Tonry J. L. et al., 2018, PASP, 130, 064505
van den Heuvel E. P. J., Bhattacharya D., Nomoto K., Rappaport S. A., 1992, A&A, 262, 97
Walker M. F., 1954, PASP, 66, 230
Warner B., 1995, Cambridge Astrophysics Series, Vol. 28. Cambridge University Press, Cambridge
Wei J. Y., Xu D. W., Qiao Q. Y., Qiu Y. L., Hu J. Y., 1999, IAU Circ., 7209, 2
Weldrake D. T. F., de Blok W. J. G., Walter F., 2003, MNRAS, 340, 12
Williams R. E., 1992, AJ, 104, 725
Williams R. E., 1994, ApJ, 426, 279
Williams R., 2012, AJ, 144, 98
Williams S. C., Darnley M. J., 2017, Astron. Telegram, 10630
Williams S. C., Darnley M. J., Bode M. F., Keen A., Shafter A. W., 2014, ApJS, 213, 10
Williams S. C., Darnley M. J., Bode M. F., Shafter A. W., 2016, ApJ, 817, 143
Williams S. C., Darnley M. J., Henze M., 2017, MNRAS, 472, 1300
Yaron O., Prialnik D., Shara M. M., Kovetz A., 2005, ApJ, 623, 398
Zwicky F., 1936, PASP, 48, 191

APPENDIX A: PHOTOMETRY OF AT 2017FVZ

In Table A1 we provide the optical photometry of AT 2017fvz from the LT and ASAS-SN. Table A2 lists the photometry of AT 2017fvz from KAIT. Table A3 presents the ATLAS photometry of AT 2017fvz.

Table A1. LT and ASAS-SN optical photometry of AT 2017fvz.

UT Date	MJD (d)	$t - t_0$ (d)	Telescope and instrument	Exposure time (s)	Filter	Photometry (mag)
2017-08-09.916	57974.916	8.032	LT IO:O	60	u'	18.522 ± 0.118
2017-08-15.908	57980.908	14.024	LT IO:O	60	u'	18.737 ± 0.063
2017-08-17.894	57982.894	16.010	LT IO:O	60	u'	19.248 ± 0.131
2017-08-19.910	57984.910	18.026	LT IO:O	60	u'	19.337 ± 0.111
2017-08-23.889	57988.889	22.005	LT IO:O	60	u'	19.633 ± 0.127
2017-08-30.883	57995.883	28.999	LT IO:O	120	u'	20.265 ± 0.191
2017-09-04.939	58000.939	34.055	LT IO:O	120	u'	20.722 ± 0.335
2017-09-19.936	58015.936	49.052	LT IO:O	120	u'	20.378 ± 0.158
2017-09-24.896	58020.896	54.012	LT IO:O	120	u'	20.571 ± 0.274
2017-10-17.842	58043.842	76.958	LT IO:O	120	u'	21.228 ± 0.131
2017-11-12.822	58098.822	102.938	LT IO:O	120	u'	21.895 ± 0.270
2017-08-09.917	57974.917	8.033	LT IO:O	60	B	18.224 ± 0.019
2017-08-15.910	57980.910	14.026	LT IO:O	60	B	19.003 ± 0.025
2017-08-17.895	57982.895	16.011	LT IO:O	60	B	19.198 ± 0.032
2017-08-19.911	57984.911	18.027	LT IO:O	60	B	19.380 ± 0.038
2017-08-23.890	57988.890	22.006	LT IO:O	60	B	19.903 ± 0.049
2017-08-30.885	57995.885	29.001	LT IO:O	120	B	20.204 ± 0.086
2017-09-04.941	58000.941	34.057	LT IO:O	120	B	19.987 ± 0.081
2017-09-19.941	58015.941	49.057	LT IO:O	120	B	20.591 ± 0.072
2017-09-24.901	58020.901	54.017	LT IO:O	120	B	20.875 ± 0.106
2017-10-17.847	58043.847	76.963	LT IO:O	120	B	21.066 ± 0.059
2017-11-12.827	58098.827	102.943	LT IO:O	120	B	21.321 ± 0.071
2017-08-03.190	57968.190	1.306	ASAS-SN	270	V	16.654
2017-08-09.918	57974.918	8.034	LT IO:O	60	V	17.905 ± 0.017
2017-08-15.911	57980.911	14.027	LT IO:O	60	V	18.722 ± 0.017
2017-08-17.896	57982.896	16.012	LT IO:O	60	V	19.035 ± 0.029
2017-08-19.912	57984.912	18.028	LT IO:O	60	V	19.428 ± 0.045
2017-08-23.891	57988.891	22.007	LT IO:O	60	V	19.691 ± 0.048
2017-08-30.887	57995.887	29.003	LT IO:O	120	V	20.128 ± 0.073
2017-09-04.943	58000.943	34.059	LT IO:O	120	V	20.148 ± 0.097
2017-09-19.946	58015.946	49.062	LT IO:O	120	V	20.341 ± 0.061
2017-09-24.906	58020.906	54.022	LT IO:O	120	V	20.565 ± 0.092
2017-10-17.852	58043.852	76.968	LT IO:O	120	V	20.758 ± 0.056
2017-11-12.832	58098.832	102.948	LT IO:O	120	V	21.079 ± 0.077
2017-08-09.919	57974.919	8.035	LT IO:O	60	r'	17.186 ± 0.011
2017-08-15.912	57980.912	14.028	LT IO:O	60	r'	17.589 ± 0.009
2017-08-17.897	57982.897	16.013	LT IO:O	60	r'	17.729 ± 0.010
2017-08-19.913	57984.913	18.029	LT IO:O	60	r'	17.886 ± 0.011
2017-08-23.892	57988.892	22.008	LT IO:O	60	r'	18.212 ± 0.013
2017-08-30.889	57995.889	29.005	LT IO:O	120	r'	18.681 ± 0.023
2017-09-04.944	58000.944	34.060	LT IO:O	120	r'	18.750 ± 0.024
2017-09-19.951	58015.951	49.067	LT IO:O	60	r'	19.153 ± 0.028
2017-09-24.911	58020.911	54.027	LT IO:O	60	r'	19.255 ± 0.038
2017-10-17.857	58043.857	76.973	LT IO:O	60	r'	19.729 ± 0.030
2017-11-12.837	58098.837	102.953	LT IO:O	60	r'	20.143 ± 0.046
2017-08-09.890	57974.890	8.006	LT SPRAT	10	r'	17.391 ± 0.027
2017-08-15.915	57980.915	14.031	LT SPRAT	10	r'	17.983 ± 0.031
2017-08-19.886	57984.886	18.002	LT SPRAT	10	r'	18.268 ± 0.035
2017-08-25.874	57990.874	23.990	LT SPRAT	10	r'	17.951 ± 0.174
2017-09-11.884	58007.884	41.000	LT SPRAT	10	r'	19.286 ± 0.043
2017-09-12.865	58008.865	41.981	LT SPRAT	10	r'	19.368 ± 0.050
2017-10-10.834	58036.834	69.950	LT SPRAT	10	r'	20.040 ± 0.067
2017-08-09.920	57974.920	8.036	LT IO:O	60	i'	17.246 ± 0.021
2017-08-15.913	57980.913	14.029	LT IO:O	60	i'	18.044 ± 0.017
2017-08-17.898	57982.898	16.014	LT IO:O	60	i'	18.230 ± 0.023
2017-08-19.914	57984.914	18.030	LT IO:O	60	i'	18.496 ± 0.026
2017-08-23.893	57988.893	22.009	LT IO:O	60	i'	18.913 ± 0.030
2017-08-30.890	57995.890	29.006	LT IO:O	120	i'	19.449 ± 0.068
2017-09-04.946	58000.946	34.062	LT IO:O	120	i'	19.569 ± 0.050

Table A1 *– continued*

UT Date	MJD (d)	$t - t_0$ (d)	Telescope and instrument	Exposure time (s)	Filter	Photometry (mag)
2017-09-19.954	58015.954	49.070	LT IO:O	60	i'	19.957 ± 0.065
2017-09-24.914	58020.914	54.030	LT IO:O	60	i'	19.649 ± 0.082
2017-10-17.860	58043.860	76.976	LT IO:O	60	i'	20.378 ± 0.076
2017-11-12.840	58098.840	102.956	LT IO:O	60	i'	20.547 ± 0.095

Table A2. KAIT photometry of AT 2017fvz. The clear filter is treated as the r' band.

UT Date	MJD (d)	$t - t_0$ (d)	Telescope and instrument	Filter	Photometry (mag)
2017-08-02.384	57967.384	0.500	KAIT	Clear	17.61 ± 0.09
2017-08-03.289	57968.289	1.405	KAIT	Clear	16.44 ± 0.11
2017-08-08.211	57973.211	6.327	KAIT	Clear	16.83 ± 0.04
2017-08-09.293	57974.293	7.409	KAIT	Clear	16.87 ± 0.06
2017-08-10.370	57975.370	8.486	KAIT	Clear	17.04 ± 0.06
2017-08-11.366	57976.366	9.482	KAIT	Clear	17.22 ± 0.05
2017-08-12.369	57977.369	10.485	KAIT	Clear	17.22 ± 0.04
2017-08-13.362	57978.362	11.478	KAIT	Clear	17.41 ± 0.05
2017-08-14.362	57979.362	12.478	KAIT	Clear	17.48 ± 0.05
2017-08-15.360	57980.360	13.476	KAIT	Clear	17.57 ± 0.04
2017-08-16.355	57981.355	14.471	KAIT	Clear	17.66 ± 0.04
2017-08-17.337	57982.337	15.453	KAIT	Clear	17.68 ± 0.09
2017-08-18.347	57983.347	16.463	KAIT	Clear	17.82 ± 0.10
2017-08-19.339	57984.339	17.455	KAIT	Clear	17.88 ± 0.05
2017-08-20.334	57985.334	18.450	KAIT	Clear	17.95 ± 0.06
2017-08-22.333	57987.333	20.449	KAIT	Clear	18.13 ± 0.07
2017-08-23.335	57988.335	21.451	KAIT	Clear	18.19 ± 0.13
2017-08-24.316	57989.316	22.432	KAIT	Clear	18.31 ± 0.07
2017-08-25.336	57990.336	23.452	KAIT	Clear	18.33 ± 0.06
2017-08-26.339	57991.339	24.455	KAIT	Clear	18.41 ± 0.09
2017-08-27.307	57992.307	25.423	KAIT	Clear	18.42 ± 0.06
2017-08-28.320	57993.320	26.436	KAIT	Clear	18.61 ± 0.06
2017-08-29.291	57994.291	27.407	KAIT	Clear	18.74 ± 0.15
2017-08-30.278	57995.278	28.394	KAIT	Clear	18.47 ± 0.22
2017-08-31.284	57996.284	29.400	KAIT	Clear	18.62 ± 0.17

Table A3. Photometry of AT 2017fvz from ATLAS observations.[a]

UT Date[b]	MJD (d)	$t - t_0$ (d)	Telescope and instrument	Filter	Photometry (mag)[c]
2017-08-03.389	57968.389	1.505 ± 0.005	ATLAS	Orange	16.511 ± 0.095
2017-08-04.440	57969.440	2.556 ± 0.006	ATLAS	Orange	16.219 ± 0.036
2017-08-09.455	57974.455	7.571 ± 0.005	ATLAS	Orange	16.955 ± 0.068
2017-08-11.436	57976.436	9.552 ± 0.005	ATLAS	Orange	17.315 ± 0.032
2017-08-12.412	57977.412	10.528 ± 0.005	ATLAS	Orange	17.447 ± 0.023
2017-08-13.446	57978.446	11.562 ± 0.005	ATLAS	Orange	17.502 ± 0.015
2017-08-15.424	57980.424	13.540 ± 0.005	ATLAS	Orange	17.520 ± 0.031
2017-08-18.399	57983.399	16.515 ± 0.005	ATLAS	Orange	17.958 ± 0.098
2017-08-22.384	57987.384	20.500 ± 0.005	ATLAS	Orange	18.209 ± 0.241
2017-08-23.405	57988.405	21.521 ± 0.005	ATLAS	Orange	18.544 ± 0.319
2017-08-26.394	57991.394	24.510 ± 0.004	ATLAS	Orange	20.143 ± 0.239
2017-08-28.370	57993.370	26.486 ± 0.004	ATLAS	Orange	19.877 ± 0.118
2017-08-16.394	57981.394	14.510 ± 0.005	ATLAS	Cyan	18.750 ± 0.169
2017-08-17.417	57982.417	15.533 ± 0.005	ATLAS	Cyan	18.519 ± 0.442
2017-08-21.411	57986.411	19.527 ± 0.010	ATLAS	Cyan	18.134 ± 0.410
2017-09-17.329	58013.329	46.445 ± 0.004	ATLAS	Cyan	20.376 ± 0.403

[a]The 'orange' filter covers the r' and i' bands. The 'cyan' filter covers the V and r' bands.
[b]The date listed here is the mean time of multiple observations taken on this date.
[c]The magnitude listed here is the mean magnitude calculated from multiple observations taken on this date with the associated standard uncertainty.

This paper has been typeset from a TEX/LATEX file prepared by the author.